Novel electron scattering experiment finds a smaller proton radius

W. Xiong[1], A. Gasparian[2†], H. Gao[1,3‡], D. Dutta[4‡*], M. Khandaker[5‡], N. Liyanage[6], E. Pasyuk[7], C. Peng[1], X. Bai[6], L. Ye[4], K. Gnanvo[6], C. Gu[1], M. Levillain[2], X. Yan[1], D. W. Higinbotham[7], M. Meziane[1], Z. Ye[1,8], K. Adhikari[4], B. Aljawrneh[2], H. Bhatt[4], D. Bhetuwal[4], J. Brock[7], V. Burkert[7], C. Carlin[7], A. Deur[7], D. Di[6], J. Dunne[4], P. Ekanayaka[4], L. El-Fassi[4], B. Emmich[4], L. Gan[9], O. Glamazdin[10], M. L. Kabir[4], A. Karki[4], C. Keith[7], S. Kowalski[11], V. Lagerquist[12], I. Larin[13,14], T. Liu[1], A. Liyanage[15], J. Maxwell[7], D. Meekins[7], S. J. Nazeer[15], V. Nelyubin[6], H. Nguyen[6], R. Pedroni[2], C. Perdrisat[16], J. Pierce[7], V. Punjabi[17], M. Shabestari[4], A. Shahinyan[18], R. Silwal[11], S. Stepanyan[7], A. Subedi[4], V. V. Tarasov[13], N. Ton[6], Y. Zhang[1] and Z. W. Zhao[1]

Elastic electron-proton scattering ($e-p$) and the spectroscopy of hydrogen atoms are the two traditional methods used to determine the proton radius (r_p). About a decade ago, a new method using muonic hydrogen (μH) atoms [1] found a significant discrepancy with the compilation of all previous results [2], creating the "proton radius puzzle." Despite intensive world-wide experimental and theoretical efforts, the "puzzle" remains unresolved. In fact, a new discrepancy between the two most recent spectroscopic measurements on ordinary hydrogen [3,4] have further deepened the mystery. Here, we report on the first high-precision $e-p$ experiment since the emergence of the "puzzle." For the first time, a magnetic-spectrometer-free method was employed, which overcame several limitations of previous $e-p$ experiments. Our result, $r_p = 0.831 \pm 0.007_{\rm stat.} \pm 0.012_{\rm syst.}$ femtometer, is significantly smaller than the last high-precision $e-p$ measurement [5] and the world average of all $e-p$ results [6]. The

†Spokesperson
‡Co-spokesperson
*Corresponding author

smaller r_p measured in our new $e-p$ experiment supports the small value found by the μH experiments. Additionally, the recently announced shift in the Rydberg constant [7], one of the best-known fundamental constants in physics, agrees with our finding.

The proton is the dominant ingredient of visible matter in the Universe. Consequently, determining the proton's basic properties such as its root-mean-square (RMS) charge radius, r_p, has attracted tremendous interest in its own right. Accurate knowledge of r_p is also required for precise calculations of the energy levels and transition energies of the hydrogen (H) atom, for example, the Lamb shift. The extended proton charge distribution changes the Lamb shift by as much as 2% [1] in the case of μH atoms, where the electron in the H atom is replaced by a "heavier electron", the muon. This makes r_p essential for the precise determination of fundamental constants such as the Rydberg constant (R_∞) [2]. The first principles calculation of r_p in the accepted theory of the strong interaction - Quantum Chromodynamics (QCD), is notoriously challenging and currently cannot reach the accuracy demanded by experiments, but, Lattice QCD calculations are on the cusp of becoming precise enough to be tested experimentally [8]. Therefore, precision measurement of r_p is critical for addressing the "proton radius puzzle" and also important for determining fundamental constants of physics and for testing lattice QCD.

Prior to 2010 the two most popular methods used to measure r_p were: (i) $ep \to ep$ elastic scattering measurements, where the slope of the extracted electric form factor (G_E^p) down to zero 4-momentum transfer squared (Q^2), is directly proportional to r_p; and (ii) Lamb shift (spectroscopy) measurements of "regular" H atoms, which, along with state-of-the-art calculations, were used to

determine r_p. Although, the $e-p$ results can be somewhat less precise than the spectroscopy results, the value of r_p obtained from these two methods [2,5] mostly agreed with each other [9]. New results based on Lamb shift measurements in μH, a newly developed spectroscopy technique, were reported for the first time in 2010. The Lamb shift in μH is several million times more sensitive to r_p because the muon is about 200 times closer to the proton than the electron in a H atom. To the surprise of both the nuclear and atomic physics communities, the two μH results [1,10] with their unprecedented, $<0.1\%$ precision, were a combined eight-standard deviations smaller than the average value from all previous experiments. This triggered the *"proton radius puzzle"* [11], unleashing intensive experimental and theoretical efforts aimed at resolving this "puzzle".

The discrepancy between r_p measured in H and μH atoms remains unresolved. Moreover, the two most recent H Lamb shift measurements disagree with each other [3,4], which has added a new dimension to and renewed the urgency of this problem. A fundamental difference between the $e-p$ and $\mu-p$ interactions, could be the origin of the discrepancy. However, there are abundant experimental constraints on any such "new physics," and yet models that resolve the puzzle with new force carriers have been proposed [11,12]. On the other hand, more mundane solutions continue to be explored, for example, the definition of r_p used in all three major experimental approaches has been rigorously shown to be consistent [13]. The effect of two-photon exchange on μH spectroscopy [14,15] and form factor nonlinearities in $e-p$ scattering [16–18] has also been examined. None of these studies could adequately explain the "puzzle" and have reinforced the need for additional high-precision measurements of r_p, using new techniques with different systematics.

The PRad collaboration at Jefferson Lab developed and performed a new $e-p$ experiment as an independent measurement of r_p, to address this "puzzle." The PRad experiment, in contrast with previous $e-p$ experiments, was designed to use a magnetic-spectrometer-free, calorimeter based method [19]. The innovative design of the PRad experiment enabled three major improvements over previous $e-p$ experiments: (i) The large angular acceptance ($0.7^\circ - 7.4^\circ$) of the hybrid calorimeter (HyCal) allowed for a large Q^2 coverage spanning two orders of magnitude ($10^{-4} - 0.06$) $(\mathrm{GeV/c})^2$, in the low Q^2 range. The single fixed location of HyCal eliminated the multitude of normalization parameters that plague magnetic spectrometer based experiments, where the spectrometer must be physically moved to many different angles to cover the desired range in Q^2. In addition, the PRad experiment reached extreme forward scattering angles down to 0.7° achieving the lowest $Q^2 \sim (10^{-4})$ $(\mathrm{GeV/c})^2$ in $e-p$ experiments, an order of magnitude lower than previously achieved. Reaching a lower Q^2 range is critically important since r_p is extracted as the slope of the measured $G_E^p(Q^2)$ at $Q^2 = 0$. (ii) The extracted $e-p$ cross sections were normalized to the well known quantum electrodynamics process - $e^-e^- \rightarrow e^-e^-$ Møller scattering from the atomic electrons ($e-e$)- which was measured simultaneously with the $e-p$ within the same detector acceptance. This leads to a significant reduction in the systematic uncertainties of measuring the $e-p$ cross sections. (iii) The background generated from the target windows, one of the dominant sources of systematic uncertainty for all previous $e-p$ experiments, is highly suppressed in the PRad experiment.

The PRad experimental apparatus consisted of the following four main elements (Figure 1): (i) a 4 cm long, windowless, cryo-cooled hydrogen (H_2) gas flow target with a thickness of

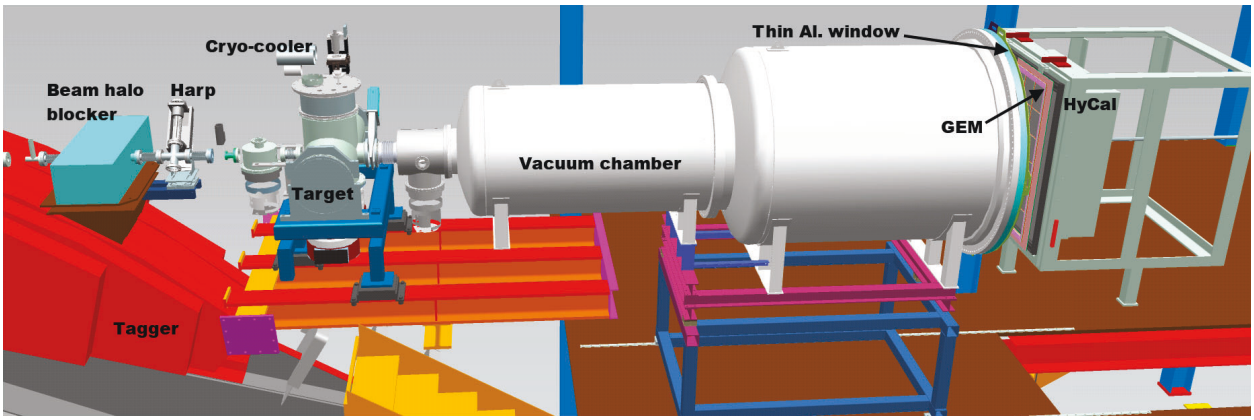

Figure 1: Schematic layout of the PRad experimental setup in Jefferson Lab, Hall B (see the text for description of individual detectors and components).

2.5×10^{18} atoms/cm^2. It eliminated the beam-background from the target windows and was the first such target used in these types of experiments; (ii) the high resolution, large acceptance HyCal electromagnetic calorimeter [20] consisting of two types of detectors, 576 Pb-glass modules and 1152 $PbWO_4$ crystal modules. The calorimeter was located 5.5 m from the target and was used to detect the forward scattered electrons. The complete azimuthal coverage of HyCal for the forward scattering angles allowed simultaneous detection of the pair of electrons from $e - e$ scattering, for the first time in these types of measurements; (iii) one plane made of two high resolution $X - Y$ gas electron multiplier (GEM) coordinate detectors located in front of HyCal; and (iv) a two-section vacuum chamber spanning the 5.5 m distance from the target to the detectors.

The PRad experiment was performed in Hall B at Jefferson Lab in May-June of 2016, using 1.1 GeV and 2.2 GeV electrons from the CEBAF accelerator. The standard Hall B beam line, designed for low beam currents (0.1-50 nA), was used in this experiment. The incident electrons that

scattered off the target protons and the Møller electron pairs, were detected in the GEM and HyCal detectors. The energy of the detected electron(s) was measured by HyCal, while the transverse $(X - Y)$ position was measured by the GEM detector, which was used to calculate the Q^2 for each detected event. The GEM detector, with a position resolution of $\sim$70 μm, improved the accuracy of Q^2 determination and allowed for an accurate determination of the detector solid angle by exploiting the kinematics constraints on the opening angle of the Møller electron pairs. Furthermore, the GEM detector suppressed the contamination from photons generated in the target and other beam line materials; the HyCal is equally sensitive to electrons and photons while the GEM is mostly insensitive to neutral particles. The GEM detector also helped suppress the position dependent irregularities in the response of electromagnetic calorimeters. A plot of the reconstructed energy versus the reconstructed angle for $e - p$ and $e - e$ events is shown in Figure 2 for the 2.2 GeV beam energy.

The background was measured every few hours with an empty target cell. To mimic the residual gas in the beam line, H_2 gas at very low pressure was allowed in the target chamber during the empty target runs. The charge normalized $e - p$ and Møller yields from the empty target cell were used to effectively subtract the background contributions. The beam current was measured with the Hall-B Faraday cup with an uncertainty of $< 0.1\%$ [21]. Further, details on the background subtraction can be found in the Supplemental Material.

A comprehensive Monte Carlo simulation of the PRad setup was developed using the Geant4 toolkit [22]. The simulation consists of two separate event generators built for the $e - p$ and $e - e$

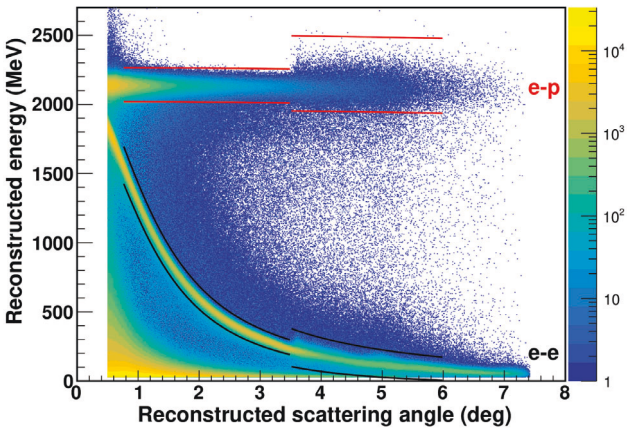

Figure 2: The reconstructed energy vs angle for $e-p$ and $e-e$ events for the electron beam energy of 2.2 GeV. The red and black lines indicate the event selection for $e-p$ and $e-e$, respectively. The angles $\leq 3.5^\circ$ are covered by the $PbWO_4$ crystals and the larger angles are covered by the Pb-glass part of HyCal.

processes. The two generators include next-to-leading order contributions to the cross section (radiative corrections), such as Bremsstrahlung, vacuum polarization, self-energy and vertex corrections. The radiative corrections to the $e-p$ and $e-e$ processes were calculated without the usual ultra relativistic approximation [23], where the mass of the electron is neglected. The two generators also include two-photon exchange processes [24], which are less than 0.2% of the $e-p$ cross section for PRad. Inelastic $e-p$ scattering events were included in the simulation using a fit [25] to the $e-p$ inelastic world data. The inelastic $e-p$ scattering contributes a background to the $e-p$ elastic spectrum which, when included enables the simulation to reproduce the measured elastic $e-p$ spectrum (see Supplementary Figure S4). The generated scattering events were propagated within the Geant4 simulation package, which included the detector geometry and materials of the PRad setup. This enabled a proper accounting of the external Bremmstrahlung of particles passing

through the intervening materials. The simulation included signal digitization and photon propagation which were critical for the precise reconstruction of the position and energy of each event in the HyCal.

The $e-p$ cross sections were obtained by comparing the simulated and measured $e-p$ yield relative to the simulated and measured $e-e$ yield. The extracted reduced cross section is shown in Figure 3**a**. At forward angles ($< 3.0^{\circ}$), where the smaller $e-e$ angular acceptance overlaps with the $e-p$ angular acceptance, the $e-p$ yield was normalized to the $e-e$ yield in each angular bin of the data. For the rest of the angular range, the $e-p$ yield for each angular bin is normalized to the integrated $e-e$ yield. The second method is applicable to the full angular range of the experiment, and the cross sections obtained using both methods were found to be consistent with each other at forward angles where they can be directly compared.

The $e-p$ elastic cross section is related to G_E^p and the proton magnetic form factor (G_M^p) as per the Rosenbluth formula [19]. In the very low Q^2 region covered by the PRad experiment, the cross section is dominated by the contribution from G_E^p. Thus, the uncertainty introduced from G_M^p is negligible. In fact, when using a wide variety of parametrizations for G_M^p [5,26–28], the extracted G_E^p varies by $\sim 0.2\%$ at $Q^2 = 0.06\ (\mathrm{GeV/c})^2$, the largest Q^2 accessed by the PRad experiment, and $< 0.01\%$ in the $Q^2 < 0.01\ (\mathrm{GeV/c})^2$ region. The largest variation in r_p arising from the choice of G_M^p parametrization is 0.001 fm. The $G_E^p(Q^2)$ extracted from our data is shown in Figure 3**b**, where the Kelly parametrization for G_M^p [26] was used.

The slope of $G_E^p(Q^2)$ as $Q^2 \rightarrow 0$ is directly proportional to r_p. A common practice is

to fit $G_E^p(Q^2)$ to a functional form and to obtain r_p by extrapolating to $Q^2 = 0$. However, each functional form truncates the higher-order moments of $G_E^p(Q^2)$ differently and introduces a model dependence which can bias the determination of r_p. It is critical to choose a robust functional form that is most likely to yield an unbiased estimation of r_p given the uncertainties in the data, and test the chosen functional form over a broad range of parametizations of $G_E^p(Q^2)$ [29]. To simultaneously minimize the possible bias in the radius extraction and the total uncertainty, various functional forms were examined for their robustness in reproducing an input r_p used to generate a mock data set. The mock data set had the same statistical uncertainty as the PRad data. The robustness was quantified in terms of the root mean square error (RMSE) defined as RMSE $= \sqrt{(\delta R)^2 + \sigma^2}$, where δR is the bias or the difference between the input and extracted radius and σ is the statistical variation of the fit to the mock data [29]. Lower order functional forms such as the monopole, dipole, and the first order expansion of Q^2 tend to give smaller uncertainties but have large biases depending on the input $G_E^p(Q^2)$ parametrization used, while higher order functional forms such as the third order Q^2 expansion and z transformation tend to give large uncertainties. These studies show [29] that consistent results with the least uncertainties can be achieved when using the multi-parameter Rational-function (referred to as Rational (1,1)):

$$f(Q^2) = nG_E(Q^2) = n\frac{1 + p_1Q^2}{1 + p_2Q^2}, \tag{1}$$

where n is the floating normalization parameter, and the charge radius is given by $r_p = \sqrt{6(p_2 - p_1)}$. The $G_E^p(Q^2)$ extracted from the 1.1 GeV and 2.2 GeV data were fitted simultaneously using the Rational (1,1) function. Independent normalization parameters n_1 and n_2 were assigned for 1.1 and 2.2 GeV data respectively, to allow for differences in normalization uncertainties, but the Q^2

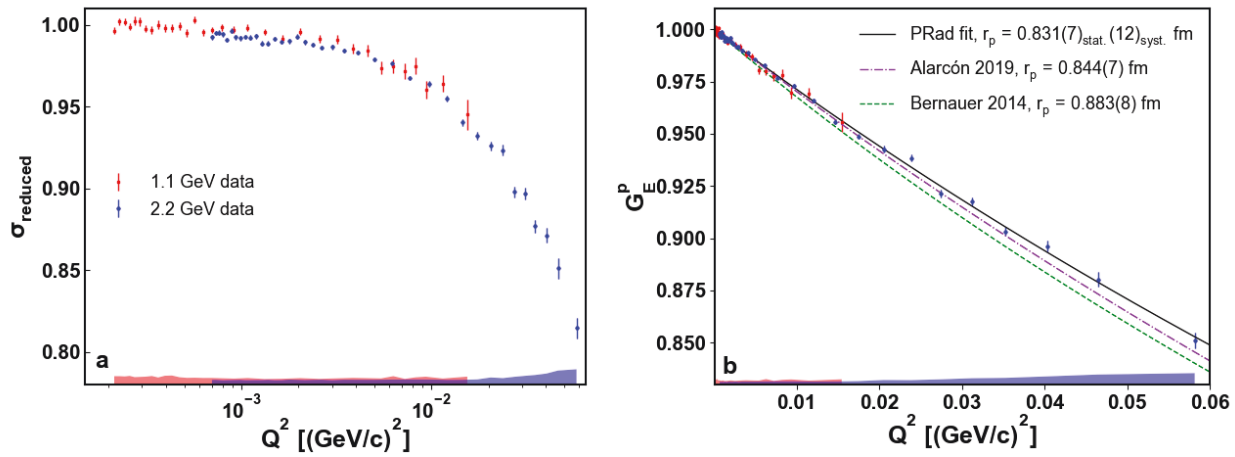

Figure 3: **a.** The reduced cross sections ($\sigma_{\text{reduced}} = \left(\frac{d\sigma}{d\Omega}\right)_{e-p} / \left[\left(\frac{d\sigma}{d\Omega}\right)_{\text{point-like}} \left(\frac{4M_p^2 E'}{(4M_p^2+Q^2)E}\right)\right]$, where E is the electron beam energy, E' is the energy of the scattered electron and M_p is the mass of the proton, for all of the PRad $e-p$ data. The systematic uncertainties are shown as bands at the bottom of the plot. **b.** The proton electric form factor as a function of Q^2. The data points are normalized with the n_1 and n_2 normalization parameters, for the 1.1 GeV and 2.2 GeV data separately. Statistical uncertainties are shown as error bars. Systematic uncertainties are shown as colored bands, for 1.1 GeV (red) and 2.2 GeV (blue). The solid black curve shows the $G_E(Q^2)$ from the fit to the function given by Eq. 1. Also shown are the fit from a previous $e-p$ experiment [5] for $r_p = 0.883(8)$ fm (green) and the calculation of Alarcon *et al.* [30] for $r_p = 0.844(7)$ fm (purple).

dependence was identical. The normalization parameters and r_p obtained from fits to the Rational (1,1) function are: $n_1 = 1.0002 \pm 0.0002_{\text{stat.}} \pm 0.0020_{\text{syst.}}$, $n_2 = 0.9983 \pm 0.0002_{\text{stat.}} \pm 0.0013_{\text{syst.}}$, and $r_p = (0.831 \pm 0.007_{\text{stat.}} \pm 0.012_{\text{syst.}})$ fm. The Rational (1,1) function describes the data very well, with a reduced χ^2 of 1.3 when considering only the statistical uncertainty. The values of r_p for a variety of functional forms fitted to the PRad data are shown in Supplementary Figure S12.

To determine the systematic uncertainty in r_p, a Monte Carlo technique was used to randomly smear the cross section and $G_E(Q^2)$ data points for each known source of systematic uncertainty. The r_p was extracted from the smeared data and the process is repeated 100,000 times. The RMS of the resulting distribution of r_p is recorded as the systematic uncertainty. The dominant systematic uncertainties of r_p are the Q^2 dependent ones which primarily affect the lowest-Q^2 data: the Møller radiative corrections, the background subtraction for the 1.1 GeV data, GEM inefficiencies, and event selection. The uncertainty of r_p arising from the finite Q^2 range and the extrapolation to Q^2 = 0, was investigated by varying the Q^2 range of the mock data set as part of the robustness study of the Rational (1,1) function [29]. This uncertainty was found to be much smaller than the statistical uncertainty ($<< 0.8\%$). The total systematic uncertainty was found to be 1.4%, and is detailed in Supplementary Table 1, and described in the Supplemental Material.

The r_p obtained using the Rational (1,1) function is shown in Figure 4, with statistical and systematic uncertainties summed in quadrature. The result is also compared with a number of previous r_p measurements. Our result obtained from Q^2 down to an unprecedented 2×10^{-4} (GeV/c)^2, is about 3-standard deviations smaller than the previous high-precision electron scattering measurement [5], which was limited to higher Q^2 (> 0.004 (GeV/c)^2). On the other hand, our result is consistent with the μH Lamb shift measurements[1,10], and also the recent 2S-4P transition frequency measurement using ordinary H atoms [3]. Given that the lowest Q^2 reached in the PRad experiment is an order of magnitude lower than the previous $e-p$ experiments, and the careful management and reduction of systematic effects, our result indicates that the proton is indeed smaller than the previously accepted value from $e-p$ measurements. Our result does not support

any fundamental difference between the $e-p$ and $\mu-p$ interactions and is consistent with the shift in the Rydberg constant announced by CODATA [7].

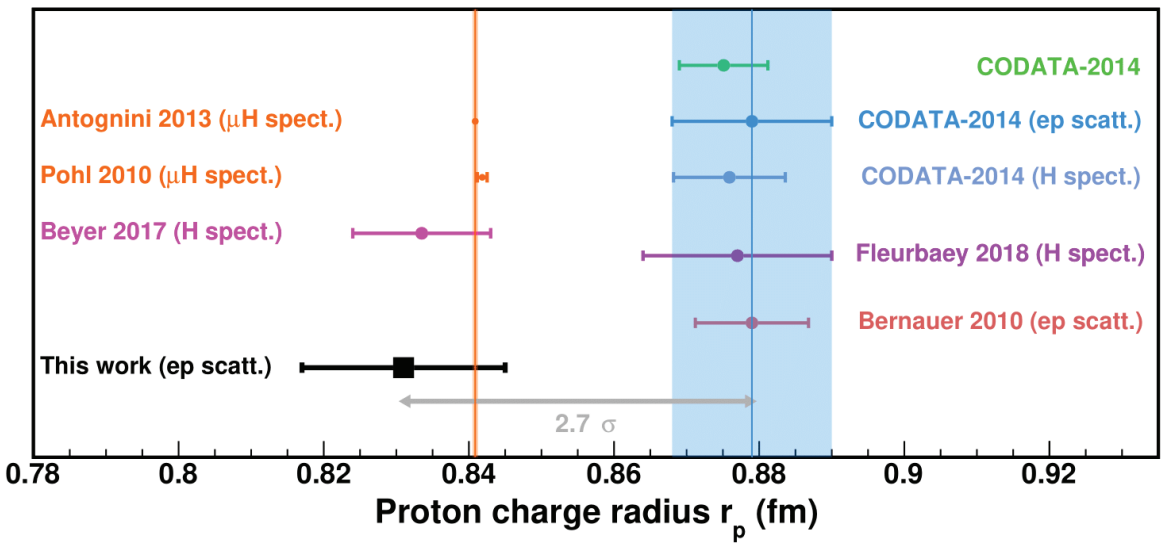

Figure 4: The r_p extracted from the PRad data, shown along with the other measurements of r_p since 2010 and the CODATA recommended values.The PRad result is 2.7-σ smaller than the CODATA recommended value for $e-p$ experiments [6].

The PRad experiment is the first $e-p$ experiment to cover a two orders of magnitude span of Q^2, in one setting. The experiment also exploited the simultaneous detection of $e-p$ and $e-e$ scattering to achieve superior control of systematic uncertainties, which were by design very different from previous $e-p$ experiments. Further, the extraction of r_p by employing functional forms with carefully validated robustness is another strength of this result. Our result introduces a large discrepancy with the previous high-precision $e-p$ experiments. On the other hand, the results also imply that there is consistency between proton charge radii obtained from regular and muonic hydrogen [1,10] and that the value of r_p is consistent with the recently updated CODATA

value [7]. The PRad experiment demonstrates the clear advantages of the calorimeter based method for extracting r_p from $e-p$ experiments and points to further possible improvements in the accuracy of this method. It also validates the recently announced shift in the Rydberg constant [7], which has profound consequences, given that the Rydberg constant is one of the most precisely known constants of physics.

1. Pohl, R. *et al*. The size of the proton. *Nature* **466**, 213–217 (2010).

2. Mohr, P. J., Taylor, B. N. & Newell, D. B. CODATA recommended values of the fundamental physical constants: 2006. *Rev. Mod. Phys.* **80**, 633–730 (2008).

3. Beyer, A. *et al*. The Rydberg constant and proton size from atomic hydrogen. *Science* **358**, 79–86 (2017).

4. Fleurbaey, H. *et al*. New measurement of the 1s-3s transition frequency of hydrogen: Contribution to the proton charge radius puzzle. *Phys. Rev. Lett.* **120**, 183001 (2018).

5. Bernauer, J. C. *et al*. High-precision determination of the electric and magnetic form factors of the proton. *Phys. Rev. Lett.* **105**, 242001 (2010).

6. Mohr, P. J., Newell, D. B. & Taylor, B. N. CODATA recommended values of the fundamental physical constants: 2014. *J. of Phys. and Chem. Ref. Data* **45**, 043102 (2016).

7. Mohr, P. J., Newell, D. B. & Taylor, B. N. CODATA recommended values of the fundamental physical constants: 2018. `http://physics.nist.gov/constants` (2019).

8. Hasan, N. *et al*. Computing the nucleon charge and axial radii directly at $q^2 = 0$ in lattice qcd. *Phys. Rev. D* **97**, 034504 (2018).

9. Mohr, P. J., Taylor, B. N. & Newell, D. B. CODATA recommended values of the fundamental physical constants: 2010. *Rev. Mod. Phys.* **84**, 1527–1605 (2012).

10. Antognini, A. *et al*. Proton structure from the measurement of 2S-2P transition frequencies of muonic hydrogen. *Science* **339**, 417–420 (2013).

11. Carlson, C. E. The proton radius puzzle. *Prog. Part. Nucl. Phys.* **82**, 59–77 (2015).

12. Liu, Y. S. & Miller, G. A. Validity of the weizsäcker-williams approximation and the analysis of beam dump experiments: Production of an axion, a dark photon, or a new axial-vector boson. *Phys. Rev. D* **96**, 016004 (2017).

13. Miller, G. A. Defining the proton radius: a unified treatment. *Phys. Rev. C* **99**, 035202 (2019).

14. Miller, G. A. Proton polarizability contribution: Muonic hydrogen lamb shift and elastic scattering. *Phys. Lett. B* **718**, 1078–1082 (2013).

15. Antognini, A. *et al*. Theory of the 2S–2P Lamb shift and 2S hyperfine splitting in muonic hydrogen. *Annals Phys.* **331**, 127–145 (2013).

16. Lee, G., Arrington, J. R. & Hill, R. J. Extraction of the proton radius from electron-proton scattering data. *Phys. Rev. D* **92**, 013013 (2015).

17. Higinbotham, D. W. *et al*. Proton radius from electron scattering data. *Phys. Rev. C* **93**, 055207 (2016).

18. Griffioen, K., Carlson, C. & Maddox, S. Consistency of electron scattering data with a small proton radius. *Phys. Rev. C* **93**, 065207 (2016).

19. Gasparian, A., Khandaker, M., Gao, H. & Dutta, D. A proposal for Jefferson Laboratory: High Precision Measurement of the Proton Charge Radius (2011). JLab PAC40 proposal.

20. Gasparian, A. A high performance hybrid electromagnetic calorimeter at jefferson lab. In C. Cecchi, P. L., P. Cenci & Pepe, M. (eds.) *Proc. XI Int. Conf. Calorim. Part. Phys.*, 109–115 (World Scientific, Singapore, 2005).

21. Mecking, B. *et al*. The CEBAF large acceptance spectrometer (CLAS). *Nucl. inst. and Meth. A* **503**, 513–553 (2003).

22. Agostinelli, S. *et al*. GEANT4: A simulation toolkit,. *Nucl. Inst. and Meth. A* **506**, 250–303 (2003).

23. Akushevich, I., Gao, H., Ilyichev, A. & Meziane, M. Radiative corrections beyond the ultra relativistic limit in unpolarized ep elastic and møller scatterings for the prad experiment at jefferson laboratory,. *Eur. Phys. J. A* **51**, 2015–1500 (2015).

24. Tomalak, O. Two-photon exchange correction in elastic lepton-proton scattering. *Few Body Syst.* **59**, 87 (2018).

25. Christy, M. E. & Bosted, P. E. Empirical fit to precision inclusive electron-proton cross-sections in the resonance region. *Phys. Rev. C* **81**, 055213 (2010).

26. Kelly, J. J. Simple parametrization of nucleon form factors. *Phys. Rev. C* **70**, 068202 (2004).

27. Venkat, S., Arrington, J., Miller, G. A. & Zhan, X. Realistic transverse images of the proton charge and magnetic densities. *Phys. Rev. C* **83**, 015203 (2011).

28. Higinbotham, D. W. & McClellan, R. E. How analytic choices can affect the extraction of electromagnetic form factors from elastic electron scattering cross section data. *arXiv:1902.08185* (2018).

29. Yan, X. *et al*. Robust extraction of the proton charge radius from electron-proton scattering data. *Phys. Rev. C* **98**, 025204 (2018).

30. Alarcon, J. M., Higinbotham, D. W., Weiss, C. & Ye, Z. Proton charge radius from electron scattering data using dispersively improved chiral effective field theory. *Phys. Rev. C* **99**, 044303 (2019).

31. Sober, I. *et al*. The bremsstrahlung tagged photon beam in hall b at jlab. *Nucl. Instr. Meth. A* **440**, 263–284 (2000).

32. Tomalak, O. & Vanderhaeghen, M. Two-photon exchange correction in elastic unpolarized electron-proton scattering at small momentum transfer. *Phys. Rev. D* **93**, 013023 (2016).

33. Tomalak, O. & Vanderhaeghen, M. Subtracted dispersion relation formalism for the two-photon exchange correction to elastic electron-proton scattering: Comparison with data. *Eur. Phys. J. A* **51**, 24 (2015).

34. Gramolin, A. V. *et al*. A new event generator for the elastic scattering of charged leptons on proton. *J. Phys. G* **41**, 115001 (2014).

35. Arrington, J. Implications of the discrepancy between proton form-factor measurements. *Phys. Rev. C* **69**, 022201 (2004).

36. Arrington, J. & Sick, I. Precise determination of low-q nucleon electromagnetic form factors and their impact on parity-violating e-p elastic scattering. *Phys. Rev. C* **76**, 035201 (2007).

37. Bernauer, J. C. *Measurement of the Elastic Electron-proton Cross Section and Separation of the Electric and Magnetic Form Factor in the Q2 Range from 0.004 to 1 (GeV/c)2* (Ph.D. Thesis, Inst. Kernphys, Johannes Gutenbeg-Universitat, Mainz, Garmany., 2010).

38. Lee, G., Arrington, J. R. & Hill, R. J. Extraction of the proton radius from electron-proton scattering data. *Phys. Rev. D* **92**, 013013 (2015).

39. Bernauer, J. C. *et al*. Electric and magnetic form factors of the proton. *Phys. Rev. C* **90**, 015206 (2014).

40. Drechsel, D., Kamalov, S. S. & Tiator, L. Unitary isobar model - maid2007. *Eur. Phys. J. A* **34**, 69 (2007).

41. Arbuzov, A. A. & Kopylova, T. V. On higher order radiative corrections to elastic electron-proton scattering. *Eur. Phys. J. C.* **75**, 603 (2015).

Affiliations

[1] *Duke University, Durham , NC 27708, USA*

[2] *North Carolina A & T State University, Greensboro, NC 27424 , USA*

[3] *Triangle University Nuclear Laboratory, Durham, NC 27708, USA*

[4] *Mississippi State University, Mississippi State, MS 39762, USA*

[5] *Idaho State University, Pocatello, ID 83209, USA*

[6] *University of Virginia, Charlottesville, VA 22904, USA*

[7] *Thomas Jefferson National Accelerator Facility, Newport News, VA 23606, USA*

[8] *Argonne National Lab, Lemont, IL 60439, USA*

[9] *University of North Carolina, Wilmington, NC 28402, USA*

[10] *Kharkov Institute of Physics and Technology, Kharkov 61108, Ukraine*

[11] *Massachusetts Institute of Technology, Cambridge, MA 02139, USA*

[12] *Old Dominion University, Norfolk, VA 23529 , USA*

[13] *Alikhanov Institute for Theoretical and Experimental Physics NRC "Kurchatov Institute", Moscow, 117218, Russia*

[14] *University of Massachusetts, Amherst, MA 01003, USA*

[15] *Hampton University, Hampton, VA 23669, USA*

[16] *College of William and Mary, Williamsburg, VA 23185, USA*

[17] *Norfolk State University, Norfolk, VA 23504, USA*

[18] *Yerevan Physics Institute, Yerevan 0036, Armenia*

Acknowledgements

This work was funded in part by the National Science Foundation (NSF MRI PHY-1229153) and by the U.S. Department of Energy (Contract No. DE-FG02-03ER41231), including contract No. DE-AC05-06OR23177 under which Jefferson Science Associates, LLC operates Thomas Jefferson National Accelerator Facility, and by the U.S. We wish to thank the staff of Jefferson Lab for their vital support throughout the experiment. We are also grateful to all granting agencies for providing funding support to the authors throughout this project. We acknowledge fruitful discussions about radiative corrections with A. Afanasev, I. Akushevich, A. V. Gramolin and O. Tomalak. We thank S. Danagoulian for helping restore the light monitoring system of HyCal. We also thank S. Javalkar for help with a beam halo study.